

## Neutron hole states in $^{89}\text{Zr}$ via the $(\vec{p}, d)$ reaction at 58 MeV

G. Duhamel-Chrétien, G. Perrin, C. Perrin, and V. Comparat

*Institut des Sciences Nucléaires, IN2P3-CNRS/Université Joseph Fourier, 53 avenue des Martyrs,  
F-38026 Grenoble CEDEX, France*

E. Gerlic and S. Galès

*Institut de Physique Nucléaire, IN2P3-CNRS/Université Paris Sud, F-91405 Orsay CEDEX, France*

C. P. Massolo

*Departemento de Fisica, Universidad de la Plata, 1900 La Plata, Argentina*

(Received 5 July 1990)

Differential cross-section and vector analyzing-power angular distributions were measured at  $E_{\vec{p}} = 58$  MeV for the  $^{90}\text{Zr}(\vec{p}, d)^{89}\text{Zr}$  reaction in the angular range from  $6^\circ$  to  $50^\circ$  and up to 10 MeV excitation energy, with 80 keV energy resolution. In addition to the transitions to low-lying states, the spectra display strong clusters of states from  $E_x = 3.5$  to 7 MeV. The observed fine structure was used to define energy bins for which cross sections and analyzing powers were obtained. The latter allowed spin and parity assignments for deep-lying hole states. Spectroscopic factors were deduced from standard distorted-wave Born approximation calculations. From the vector analyzing-power measurements, it was shown that most of the strength observed above 3.5 MeV belongs to the  $1f_{7/2}$  inner neutron hole orbital.

### I. INTRODUCTION

One-nucleon transfer reactions have been extensively used over the last decade to investigate the deeply bound hole states in medium and heavy nuclei, and have allowed the location of the main contribution of high  $l$  orbital strengths belonging to the first inner shell in a number of nuclei.<sup>1</sup> Such states manifest themselves in pickup spectra as “giant-resonance-like” structures in which the hole strength is spread over many states. Unambiguous  $J$  spin determinations need measurements of vector analyzing powers, which have been shown to enable a discrimination of  $J = l - \frac{1}{2}$  and  $l + \frac{1}{2}$  transfers, for deep-lying proton hole states<sup>2,3</sup> as well as for neutron hole states.<sup>4–8</sup> Such a determination allows us to deduce less model-dependent strength functions, as well as the spin-orbit splitting between two partners belonging, respectively, to valence and inner shells. This type of model-independent analysis is required for a comparison with theoretical predictions in  $^{89}\text{Zr}$ . Recent experiments lead to rather different results concerning the  $1f_{7/2}$  and  $1f_{5/2}$  neutron hole strength distributions. In the  $^{90}\text{Zr}(^3\text{He}, \alpha)^{89}\text{Zr}$  reactions performed at 97 (Ref. 9) and 39 MeV,<sup>10</sup> respectively, about 50% of the  $1f_{7/2}$  neutron hole strength has been observed in the excitation energy range of  $E_x \simeq 3.5$ –7.7 MeV. In contrast, the  $(\vec{p}, d)$  reaction at 90 MeV (Ref. 8) showed that in this energy range the strength originates mainly from the  $1f_{5/2}$  neutron subshell, most of the  $1f_{7/2}$  strength being distributed above 7 MeV excitation energy. Moreover, the value of the  $1f$  spin-orbit splitting deduced from this  $(\vec{p}, d)$  study was about 2 MeV larger than the one deduced from the  $(^3\text{He}, \alpha)$  experiments<sup>9,10</sup> or predicted by microscopic calculations.<sup>11</sup> However, in the

$(^3\text{He}, \alpha)$  experiments, unique  $J$  assignments were not possible because unpolarized beam was used, while in the  $(\vec{p}, d)$  work the  $J$  assignment and the strength distribution were obtained for rather large energy bins (1–4 MeV width). In order to solve these discrepancies and to deduce accurate strength distribution for the  $1f_{5/2}$  and  $1f_{7/2}$  neutron hole orbitals, it appears desirable to perform experiments with good energy resolution and polarized beam.

We present in this paper the differential cross section  $\sigma(\theta)$  and vector analyzing power  $A_y(\theta)$  angular distributions obtained up to 10 MeV excitation energy in an investigation of the  $(\vec{p}, d)$  reaction at 58 MeV incident energy on a  $^{90}\text{Zr}$  target with 80 keV energy resolution. The present work was focused on the fine-structure region from 3.5 to 7 MeV, for which the discrepancies between previous experiments require a careful analysis. Unambiguous spin assignments were made by means of the asymmetry measurements  $A_y(\theta)$ , which have been compared both to empirical  $A_y(\theta)$  curves obtained for states with well-established spin and parity, and to distorted-wave Born approximation (DWBA) predictions.

### II. EXPERIMENTAL PROCEDURE

The experiment was performed using the 58 MeV polarized proton beam from the Grenoble I.S.N. cyclotron. The beam polarization was measured with a carbon polarimeter periodically inserted into the beam 0.6 m upstream from the scattering chamber. The spin direction was automatically flipped every 0.2 sec during data acquisition in order to reduce systematic errors. The polarization in both “spin-up” and “spin-down” orientations was found to be about 63%. The detailed proper-

ties of the polarized proton beam were previously reported in Ref. 12.

The target consisted of an isotopically enriched self-supporting  $^{90}\text{Zr}$  (96.33%) metallic foil with thickness of  $5.98\text{ mg/cm}^2$ . An overall energy resolution of  $80\text{ keV}$  was obtained, mainly due to the energy straggling in the target.  $^{12}\text{C}$  and Mylar foil targets were used to calibrate the position residual energy spectra in the  $^{89}\text{Zr}$  nucleus.

The outgoing deuterons were momentum analyzed in a magnetic spectrometer covering a solid angle of  $0.96\text{ msr}$  and detected in the focal plane by means of a position-sensitive multiwire proportional chamber followed by two plastic scintillators, 6 and 10 mm thick. The thickness of the first scintillator was chosen to stop the tritons, but not the deuterons. Energy-loss  $\Delta E$  signals from the two scintillators were used for particle identification. A more extensive description of the experimental setup can be found in Ref. 5. The beam current, measured in a Faraday cup, was typically about  $10\text{ nA}$ .

The differential cross sections and analyzing powers were measured from  $6^\circ$  to  $45^\circ$  laboratory angles by typically  $4^\circ$  steps. Experimental difficulties at forward angles have lead us to apply a renormalization procedure involving an additional uncertainty in the cross-section absolute values of  $\pm 20\%$  for these angles, which explains the largest error bars in the cross-section angular distributions. However, the  $A_y(\theta)$  values were not affected by this procedure. Two magnetic-field settings were required to observe states in  $^{89}\text{Zr}$  up to  $\sim 10\text{ MeV}$  excitation energy, and care was taken to ensure significant overlap between adjacent momentum bits in order to facilitate the peak identification and energy calibration of the spectra. It was achieved by using the well-known energies of the low-lying levels and first four isobaric analog states (IAS) in  $^{89}\text{Zr}$ . The relevant states are labeled with an asterisk in Table II. The uncertainties in the excitation energies resulting from this energy calibration range from  $20\text{ keV}$

for the strong transitions below  $2.2\text{ MeV}$  to about  $50\text{ keV}$  for weaker ones or more complex groups above  $2.2\text{ MeV}$ .

A  $^{89}\text{Zr}$  typical spectrum (at  $\theta_{\text{lab}}=20^\circ$ ) is shown in Fig. 1. At small angles ( $<20^\circ$ ),  $l=1$  transitions are strongly enhanced up to  $10\text{ MeV}$  excitation energy, but at larger angles,  $l=3$  and 4 states dominate the spectrum. Owing to the  $80\text{ keV}$  energy resolution, distinct levels or groups of levels can be observed in the  $3.5\text{--}7.0\text{ MeV}$  excitation energy range, superimposed on a smooth background. Above  $7\text{ MeV}$ , the spectra are rather structureless except for the sharp isobaric analog states located between  $8$  and  $10\text{ MeV}$  excitation energy. In order to obtain the background shape, spectra are recorded up to  $13\text{ MeV}$  excitation energy at three angles.

### III. DISTORTED-WAVE ANALYSIS

The experimental cross sections and analyzing powers were analyzed in the framework of the DWBA theory of direct reactions. The calculations were made using the code DWUCK 4 (Ref. 13) with local zero-range (ZR) approximation. Different sets of proton and deuteron optical parameters taken from the compilation of Perey and Perey,<sup>14</sup> or from some more recent elastic, inelastic, and transfer reaction studies,<sup>15–17</sup> were used in order to reproduce, as test cases, the data obtained for the first four known low-lying states of  $^{89}\text{Zr}$  [ $E_x=0.0\text{ MeV}$  ( $\frac{9}{2}^+$ ),  $0.595\text{ MeV}$  ( $\frac{1}{2}^-$ ),  $1.1\text{ MeV}$  ( $\frac{3}{2}^-$ ), and  $1.46\text{ MeV}$  ( $\frac{5}{2}^-$ )].

The selected potentials have also to reproduce the data for the first four IAS located at  $8.11\text{ MeV}$  ( $\frac{1}{2}^-$ ),  $9.02\text{ MeV}$  ( $\frac{9}{2}^+$ ),  $9.62\text{ MeV}$  ( $\frac{3}{2}^-$ ), and  $9.86\text{ MeV}$  ( $\frac{5}{2}^-$ ). An additional test is provided by a comparison of the strengths extracted<sup>8–10</sup> with a normalization constant  $N=2.29$ . This analysis leads to the following conclusions: (i) The different proton potentials associated with the same deuteron potentials give almost identical results in both shape and magnitude for all  $l$  transfers. (ii) For the exit

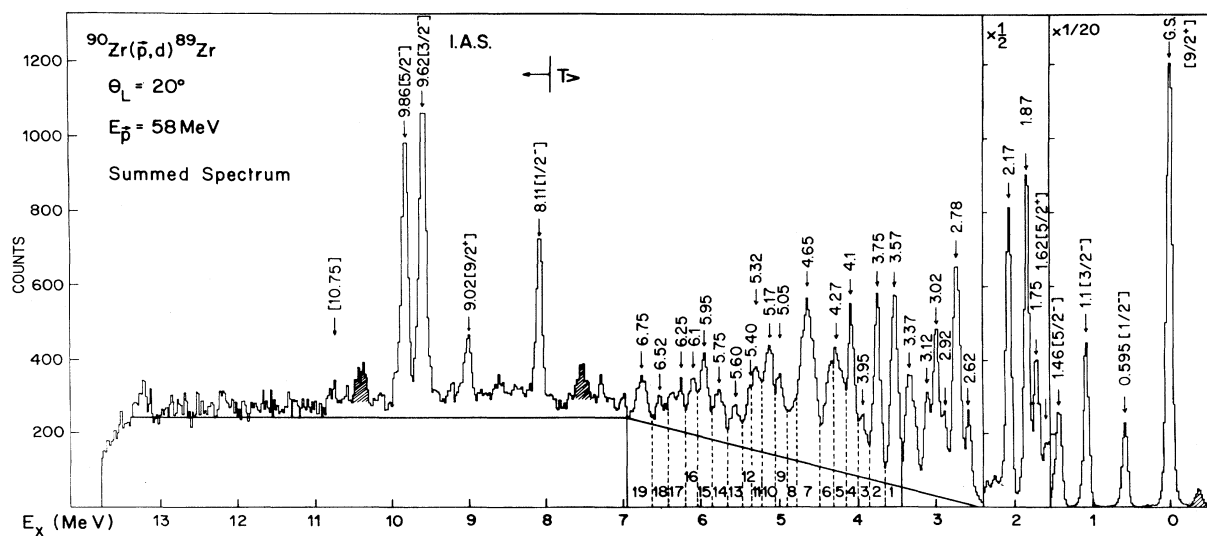


FIG. 1. Deuteron energy spectrum from the  $^{90}\text{Zr}(\bar{p}, d)^{89}\text{Zr}$  reaction recorded at  $\theta_{\text{lab}}=20^\circ$ ; the horizontal line shows our background assumption. The shaded areas are peaks due to contaminants.

TABLE I. Optical model parameters used in the analysis of the  $^{90}\text{Zr}(\vec{p},d)^{89}\text{Zr}$  reaction at  $E_{\vec{p}} = 58$  MeV.

Nucleus	Projectile	$V_r$ (MeV)	$r_r$ (fm)	$a_r$ (fm)	$W_v$ (MeV)	$W_s$ (MeV)	$r_i$ (fm)	$a_i$ (fm)	$V_{s.o.}$ (MeV)	$r_{s.o.}$ (fm)	$a_{s.o.}$ (fm)	$r_c$ (fm)
$^{90}\text{Zr}$	$p^a$	43.64	1.16	0.75	6.42	3.022	1.37	0.387	6.04	1.064	0.78	1.27
	$d^b$	98.54	1.17	0.779	6.30	$\times 4$ 12.8	1.29	0.632	$\times 4$ 6.2	1.01	0.75	1.25
	$n$	$V_n$	1.25	0.65					$\times 2$	$\lambda = 1.25$		1.3

<sup>a</sup>Reference 18.

<sup>b</sup>The so-called "adiabatic" deuteron potential has been constructed from the averaged neutron and proton parameters of Bechetti and Greenless (Ref. 19) following the prescription of Ref. 20.

channel, the adiabatic potential<sup>20</sup> is found to give the best overall fit to the cross sections for all  $l$  transfers and reproduces reasonably well the shape and magnitude of the observed analyzing powers.

The adopted set of optical parameters is listed in Table I. The comparison between experimental points and theoretical curves for the levels mentioned above are displayed in Figs. 2 and 3 for the low-lying levels and IAS

respectively. Concerning the low-lying levels, the fits to the differential cross sections are rather good. As regards the analyzing powers, the agreement is quite reasonable for all the  $l$  transfers. The  $A_y(\theta)$  experimental curves display an out-of-phase oscillatory pattern for the  $J = \frac{3}{2}^-$

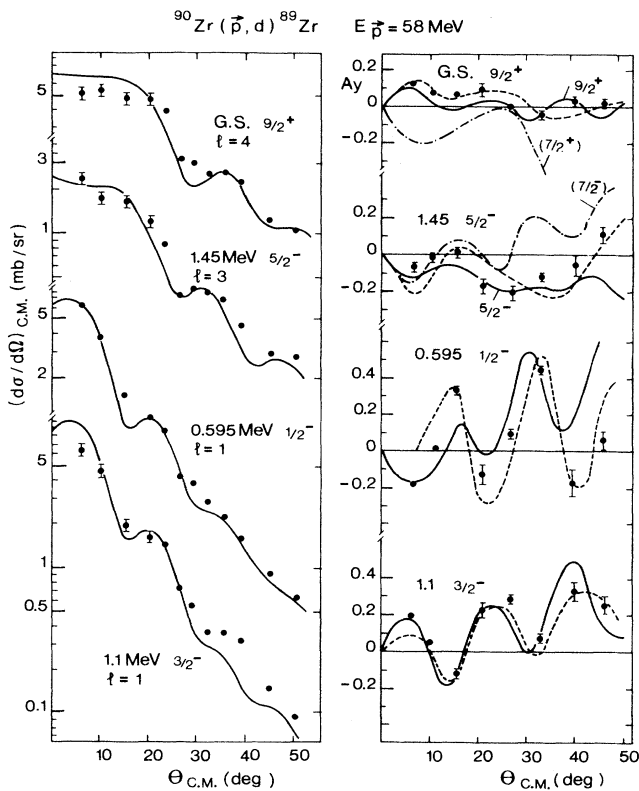


FIG. 2. Angular distributions of differential cross sections and analyzing powers for the first four well-known low-lying levels. The solid lines stand for the DWBA predictions relative to the  $J^\pi$  assignments, while the dot-dashed lines show the DWBA calculations for the corresponding spin-orbit partner. The dashed lines are empirical  $A_y(\theta)$  angular distributions taken from  $^{92}\text{Mo}(\vec{p},d)^{91}\text{Mo}$  experiment at  $E_p = 50$  MeV (Ref. 21).

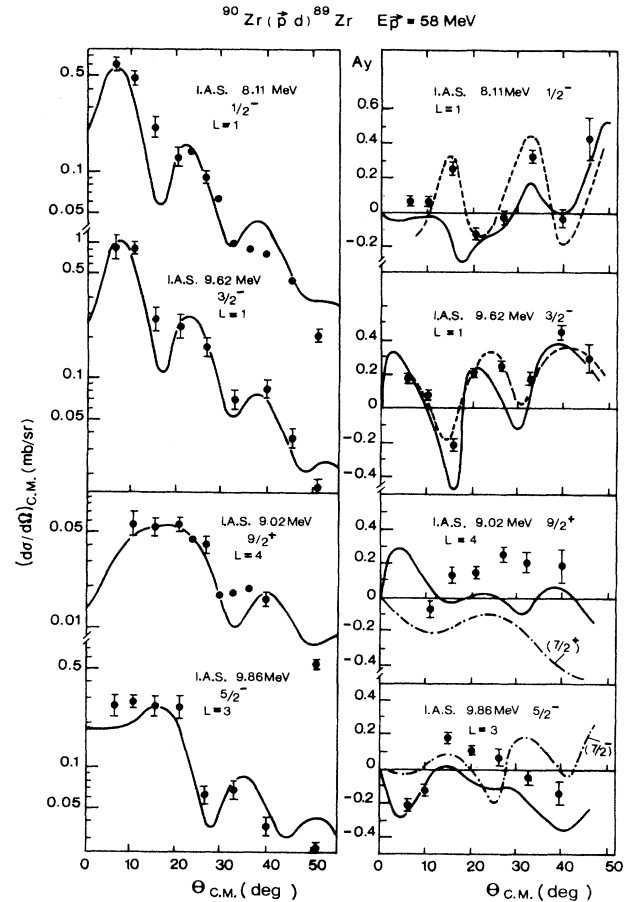


FIG. 3. Angular distributions of differential cross sections and analyzing powers for the four strongest populated  $T_>$  states (IAS), namely,  $\frac{1}{2}^-$  (8.11 MeV),  $\frac{9}{2}^+$  (9.02 MeV),  $\frac{3}{2}^-$  (9.62 MeV), and  $\frac{5}{2}^-$  (9.86 MeV). Solid and dot-dashed lines: the same as Fig. 2. Dashed lines are empirical behavior from the corresponding first low-lying  $\frac{1}{2}^-$  and  $\frac{3}{2}^-$   $T_<$  levels.

and  $\frac{1}{2}^-$  levels, both for the low-lying and isobaric analog states. For all the considered spin-orbit partners, the calculated  $A_y(\theta)$  curves show substantially different behavior with scattering angle (see Fig. 2), which allows unambiguous spin assignment. A comparison with the  $A_y(\theta)$  experimental curves (see Fig. 2) from the  $^{92}\text{Mo}(\bar{p}, d)^{91}\text{Mo}$  reaction studied at  $E_{\bar{p}} = 50$  MeV (Ref. 21) reveals similar characteristics for the  $\frac{1}{2}^-$ ,  $\frac{3}{2}^-$ ,  $\frac{5}{2}^-$ , and  $\frac{9}{2}^+$  levels. Such empirical analyzing-power curves help us to propose a definite spin assignment in the same way as in previous  $(\bar{p}, d)$  studies (see, for example, Refs. 4 and 8).

The spectroscopic factors for the low-lying levels were extracted using the usual separation energy (SE) method, which is known to give too large  $C^2S$  for IAS. For these levels, the spectroscopic factors were extracted using the effective binding-energy procedure, which gives more accurate values for such levels with large separation energies (see Table II).

The  $C^2S$  values compared with the ones obtained from previous works<sup>8-10</sup> are listed in Table II for levels up to 3.5 MeV (see Sec. IV) and in Table III for levels from 3.5 to  $\sim 7$  MeV (see Sec. V). The fragmentation and intensities of the  $l=4, 1$ , and 3 neutron hole strengths will be discussed in Sec. VI.

#### IV. EXCITATION ENERGY REGION 0–3.5 MeV

Typical differential cross sections  $\sigma(\theta)$  and analyzing-power angular distributions  $A_y(\theta)$  are shown in Fig. 4 for levels above 1.5 MeV. The extracted spectroscopic strengths are listed in Table II, together with the  $l$  transfers and spin values determined from the present work, and compared with the  $C^2S$  obtained from previous experiments. The  $1g_{9/2}$ ,  $2p_{1/2}$ ,  $2p_{3/2}$ , and  $1f_{5/2}$  valence hole strengths are found to be mostly exhausted ( $\geq 55\%$ ) by the four first levels, respectively, in agreement with previous pickup studies.<sup>8-10</sup> Some other weaker  $l=1, 3, 4$  transitions are observed in the 1.5–3.5-MeV region, which spins can be clearly assigned from the present work. These levels could correspond to fragmented states mainly due to the weak coupling of the single hole valence states with strong collective states of the  $^{90}\text{Zr}$  core such as the  $2_1^+$ ,  $5_1^-$ , or  $3_1^-$  levels at  $E_x = 2.18$ , 2.32, and 2.75 MeV, respectively.

The few  $l=1$  transitions observed in Ref. 10 above 1.5 MeV in  $^{89}\text{Zr}$  were all assumed to have spin and parity  $J^\pi = \frac{3}{2}^-$ . However, in the present study, the two  $l=1$  levels clearly identified at 1.75 and 1.87 MeV exhibit experimental  $A_y(\theta)$  completely out of phase; on the basis of

TABLE II. Spectroscopic results for low-lying levels up to 3.5 MeV and IAS in  $^{89}\text{Zr}$ . The asterisk denotes level used for the excitation energy calibration curve.

$E_x$ (MeV)	$l$	$J^\pi$ ( $\bar{p}, d$ ) This work	$C^2S$	$C^2S$ ( $^3\text{He}, \alpha$ ) (Ref. 10)	$C^2S$ ( $^3\text{He}, \alpha$ ) (Ref. 9)	$C^2S$ ( $\bar{p}, d$ ) (Ref. 8)
0*	4	$\frac{9}{2}^+$	7.1	8.0	9.1	9.6
0.595*	1	$\frac{1}{2}^-$	2.4	1.7	1.6	1.2
1.1*	1	$\frac{3}{2}^-$	2.7	2.5	2.4	2.1
1.46* <sup>a</sup>	3	$\frac{5}{2}^-$	3.0	2.5	2.7	3.5
1.62*	2	$\frac{5}{2}^+$	0.085	0.10		
1.75*	1	$\frac{1}{2}^-$	0.38		$\sum C^2S 1g_{9/2}$ =0.60	
1.87*	1	$\frac{3}{2}^-$	0.58	0.53		0.53
2.11	3	$\frac{5}{2}^-$	1.12	1.00		0.66
2.28	(4)+(1)	$(\frac{9}{2}^+)$			$\sum C^2S 2p_{1/2}$ =0.10	
2.39	(4)+(1)	$(\frac{9}{2}^+)$				
2.62	4	$\frac{9}{2}^+$	0.12	(0.11)		
2.78	$\left\{ \begin{array}{l} 3 \\ 4 \end{array} \right.$	$\left\{ \begin{array}{l} \frac{7}{2}^- \\ \frac{9}{2}^+ \end{array} \right.$	$\left\{ \begin{array}{l} 0.21 \\ 0.19 \end{array} \right.$	$\left\{ \begin{array}{l} (0.28) \\ (< 0.14) \end{array} \right.$	$\sum C^2S 2p_{3/2}$ =0.90	0.29
2.92						
3.02	3	$\frac{7}{2}^-$	0.30	(0.28)		0.46 <sup>b</sup>
3.12	4	$\frac{9}{2}^+$	0.15	(0.13)	$\sum C^2S 1f_{5/2}$ =2.10	
3.37	4	$\frac{9}{2}^+$	0.20	(0.06)		
8.11*	1	$\frac{1}{2}^-$	0.14	0.17	0.11–0.15	0.11
9.02*	4	$\frac{9}{2}^+$	0.06	0.14	0.089–0.12	0.11
9.62*	1	$\frac{3}{2}^-$	0.22	0.33	0.2–0.27	0.24
9.86*	3	$\frac{5}{2}^-$	0.41	0.71	0.5–0.67	0.64

<sup>a</sup>The contribution from the unresolved 1.52 MeV ( $\frac{9}{2}^+$ ) level calculated with  $C^2S \sim 0.37$  (see Ref. 10) has been subtracted.

<sup>b</sup>Proposed as  $J^\pi = \frac{5}{2}^-$  in Ref. 8.

DWBA calculations, these levels are unambiguously assigned as  $2p_{1/2}^{-1}$  and  $2p_{3/2}^{-1}$  fragments, respectively.

The  $l=3$  transition at  $E_x=2.11$  MeV shows negative measured  $A_y(\theta)$  values, especially between  $20^\circ$  and  $40^\circ$ , very similar to those of the 1.46 MeV ( $\frac{5}{2}^-$ ) level and is well reproduced up to  $40^\circ$  by DWBA calculations involving  $1f_{5/2}$  transfer. Experimental analyzing power of the  $^{91}\text{Mo}$  ( $\frac{5}{2}^-$ ) level at 1.53 MeV exhibits similar characteristics,<sup>21</sup> which give us additional confidence in the proposed assignment. In contrast, the  $l=3$  transition at 3.02 MeV has slightly positive or near-zero  $A_y(\theta)$  values throughout the measured angular range, qualitatively reproduced by DWBA calculations assuming  $1f_{7/2}$  transfer except around  $32^\circ$  where the predicted oscillation is not observed. In any case, such  $A_y(\theta)$  data cannot be fitted by  $\frac{5}{2}^-$  theoretical or experimental curves (see Fig. 4). This 3.02 MeV level could be identified with the suggested  $\frac{7}{2}^-$  state at 3.016 MeV observed in the  $\beta^+$  decay of  $^{89}\text{Nb}$ .<sup>22</sup>

The 2.78 MeV complex level is not reproduced by DWBA predictions including unique  $l$  transfer. The contribution from the 2.732-MeV ( $l=4$ ) state reported in Ref. 10 cannot be excluded at this level, the experimental

cross-section and analyzing-power angular distributions of which are very well fitted by an empirical mixing of  $l=3$  ( $\frac{7}{2}^-$ ) and  $l=4$  ( $\frac{9}{2}^+$ ) contributions.

In addition to the  $l=4$  ground state, which has well-established  $J^\pi=\frac{9}{2}^+$  spin and parity, other weak  $l=4$  transitions are identified between 2.5 and 3.5 MeV in  $^{89}\text{Zr}$ , which have been suggested in Ref. 10 as components of the  $1g_{9/2}^{-1}$  neutron hole orbital. In the present study, almost all the observed  $l=4$  states ( $E_x=2.62$ , 3.12, and 3.37 MeV) display similar behavior for the analyzing powers, i.e., slightly positive and rather structureless between  $6^\circ$  and  $20^\circ$ , very similar to the  $A_y(\theta)$  data for the ground state ( $\frac{9}{2}^+$ ) of  $^{89}\text{Zr}$  and  $^{91}\text{Mo}$ .<sup>21</sup> The DWBA calculations assuming  $1g_{9/2}$  transfer reproduce only qualitatively the data, but on the basis of the empirical curves the above levels have been assigned  $J^\pi=\frac{9}{2}^+$ . Moreover, two levels at 2.28 and 2.39 MeV, very weakly populated by the  $(\bar{p},d)$  reaction, have measured cross sections and analyzing powers compatible with a dominant  $J^\pi=\frac{9}{2}^+$  assignment. They could be tentatively identified with the 2.297 and 2.388 MeV states observed in the study of the  $^{89}\text{Y}(p,n\gamma)$  and  $^{86}\text{Sr}(\alpha,n\gamma)$  reactions,<sup>22</sup> and are presumably populated through a two-step pro-

TABLE III. Spectroscopic results for the deeply bound hole states (3.5–7.0 MeV) in  $^{89}\text{Zr}$ . The asterisk denotes the complex peaks.

Group <sup>a</sup>	Centroid energy (MeV)	$l$	$J^\pi$ ( $\bar{p},d$ ) This work	$C^2S$	$C^2S$ ( $^3\text{He},\alpha$ ) (Ref. 10)	$C^2S$ ( $\bar{p},d$ ) (Ref. 8)
1	3.57	3	$\frac{5}{2}^-$	0.58	0.52 <sup>b</sup>	
2	3.75	3	$\frac{5}{2}^-$	0.47	0.46 <sup>b</sup>	
3	3.95	3	$\frac{7}{2}^-$	0.14	0.15 <sup>c</sup>	} 0.82 <sup>c</sup>
4	4.1	3	$\frac{7}{2}^-$	0.28	0.43 <sup>c</sup>	
5*	4.27	3+(2)	$\frac{7}{2}^- + (\frac{5}{2}^+)$	0.25 <sup>c</sup>	0.09 <sup>c</sup>	
6	4.59	3	$\frac{7}{2}^-$	0.24	0.12 <sup>c</sup>	
7*	4.65	3+(2)	$\frac{7}{2}^- + (\frac{5}{2}^+)$	0.44 <sup>c</sup>	0.19,0.04	
8	4.85	3	$\frac{7}{2}^-$	0.19	0.12 <sup>c</sup>	
9	5.05	3	$\frac{7}{2}^-$	0.18	0.15 <sup>c</sup>	} 0.35 <sup>c</sup>
10*	5.17	3+(1)	$\frac{7}{2}^- + (\frac{3}{2}^-)$	0.28 <sup>c</sup>		
11	5.32	3+(1)	$\frac{7}{2}^- + (\frac{3}{2}^-)$	0.19 <sup>c</sup>	0.20 <sup>c</sup>	
12	5.40	3+(1)	$\frac{7}{2}^- + (\frac{3}{2}^-)$	0.14 <sup>c</sup>		
13 <sup>d</sup>	5.60	1+3	$\frac{3}{2}^- + \frac{7}{2}^-$	0.042,0.068		
14 <sup>d</sup>	5.75	1+3	$\frac{3}{2}^- + \frac{7}{2}^-$	0.04,0.069	0.11 <sup>c</sup>	
15 <sup>d</sup>	5.95	1+3	$\frac{3}{2}^- + \frac{7}{2}^-$	0.087,0.078	0.15 <sup>c</sup>	
16 <sup>d</sup>	6.1	1+3	$\frac{3}{2}^- + \frac{7}{2}^-$	0.04,0.064	0.14 <sup>c</sup>	
17 <sup>d</sup>	6.25	1+3	$\frac{3}{2}^- + \frac{7}{2}^-$	0.082,0.076	0.038 <sup>c</sup>	
18 <sup>d</sup>	6.52	1+3	$\frac{3}{2}^- + \frac{7}{2}^-$	0.04,0.066		
19*	6.75	3+(1)	$\frac{7}{2}^- + (\frac{3}{2}^-)$	0.19	0.25 <sup>c</sup>	
						$\sum C^2S 1f_{5/2}$ = 1.7

<sup>a</sup>The numbering refers to the energy bins as indicated in Fig. 1.

<sup>b</sup>If pure  $f_{5/2}$ .

<sup>c</sup>If pure  $f_{7/2}$ .

<sup>d</sup>Assuming the same yield from  $2p_{3/2}$  and  $1f_{7/2}$  at forward angles for the energy bins 13–18.

cess. Such states could be components of the  $(1g_{9/2} \times 2^+)$  multiplet, which is expected in a pure weak-coupling scheme, to lie around 2.2 MeV.

The 2.92 MeV level was interpreted in Ref. 10 as a component of the  $1g_{9/2}$  neutron hole orbital, but in this work it shows atypical cross section and analyzing-power angular distributions. None of the DWBA calculations assuming a one-step process and unique  $l$  transfer can reproduce such a behavior.

To summarize, about 88%, 90%, and 75% of the  $1g_{9/2}$ ,  $2p_{3/2}$ , and  $1f_{5/2}$   $T_{<}$  strengths are observed below 3.5 MeV, the lowest-lying fragments exhausting, respectively, 78%, 74%, and 55% of the corresponding strength. The whole  $2p_{1/2}$   $T_{<}$  strength is located in two

components. The main one contains 86% of the measured strength which already exceeds the  $2p_{1/2}$   $T_{<}$  sum rule limit by  $\sim 30\%$ . In addition, a small part of the  $1f_{7/2}$   $T_{<}$  strength ( $\sim 7\%$ ) has been observed in this energy range.

## V. DEEPLY BOUND HOLE STATES: $E_x = 3.5\text{--}7.0$ MeV

In the excitation energy range of  $E_x = 3.5\text{--}7.0$  MeV, the  $^{89}\text{Zr}$  spectra show a number of enhanced states or groups of states superimposed over a smooth background. This region was subdivided into adjacent bins (labeled by numbers 1–19) corresponding to the fine structures which could be recognized at all angles at the same excitation energy. The centroid energy of each slice is indicated in the displayed spectrum of Fig. 1. The cross sections and analyzing powers were extracted separately after subtraction of the assumed background drawn on the figure. This background corresponds to the usually adopted procedure, which consists in connecting the pronounced minima at 2.5 and 7 MeV, and extending it to higher excitation energy, so as to match the structureless background observed beyond the IAS. Figure 5 displays some typical angular distributions and analyzing-power data together with the results of DWBA calculations. The spectroscopic factors measured in this energy range are summarized in Table III. They have to be considered as a lower limit, and a different but reasonable choice of background would lead to higher  $C^2S$  value by  $\sim 15\%$ .

The experimental cross-section angular distributions of all fragmented components are consistent with a dominant  $l=3$  assignment. However, four classes of analyzing power can be observed. The first one encompasses the  $A_y(\theta)$ 's very similar to the 1.46 MeV ( $\frac{5}{2}^-$ ) level analyzing power, i.e., with negative values near  $30^\circ$ , but which can be qualitatively reproduced only up to  $35^\circ$  by DWBA calculations assuming  $1f_{5/2}$  transfer. On this basis, a  $J^\pi = \frac{5}{2}^-$  assignment is proposed for the peaks at 3.57 and 3.75 MeV.

The second includes all  $A_y(\theta)$ 's similar to the experimental analyzing powers of the 3.02 MeV level assumed to have  $J^\pi = \frac{7}{2}^-$  spin and parity (see Sec. IV), and of the 4.1 MeV level, previously assigned  $\frac{7}{2}^-$ .<sup>8</sup> DWBA calculations involving  $1f_{7/2}$  transfer give only qualitative fits to the data, the predicted peak near  $32^\circ$  not being observed. On the basis of the empirical curves, we propose a  $J^\pi = \frac{7}{2}^-$  assignment to groups 3–9, i.e., for the excitation energy range 3.85–5.10 MeV, the main contribution being concentrated between 4.0 and 4.7 MeV with about 35% of the total  $1f_{7/2}$   $T_{<}$  hole strength observed up to 7.0 MeV. However, analyzing powers of groups 5 (at  $E_x = 4.27$  MeV) and 7 (at  $E_x = 4.65$  MeV) seem better fitted by an equal-weight empirical mixture of  $1f_{7/2}$  and  $1d_{5/2}$  transitions. The weak  $l=2$  states reported in Ref. 10 at 4.36 and 4.73 MeV were not resolved in the present experiment, but they could give some contribution in these two groups. It must be pointed out that in the  $^{90}\text{Zr}(\vec{p}, d)^{89}\text{Zr}$  reaction at 90 MeV,<sup>8</sup> some  $1f_{7/2}$  strength was also reported for peaks at 4.1 and 5.2 MeV, corre-

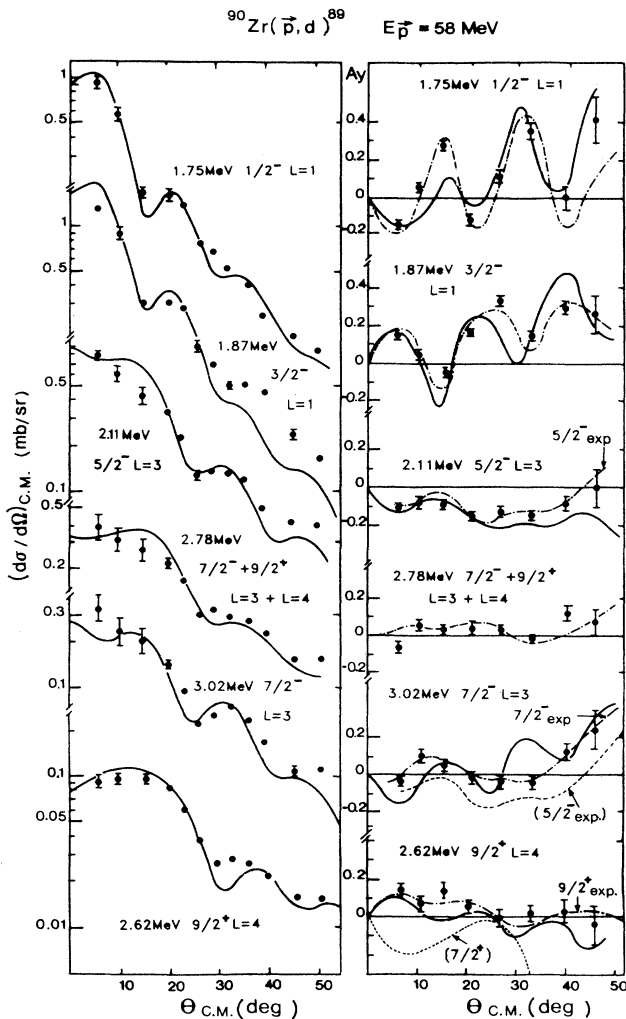


FIG. 4. Typical angular distributions of differential cross sections and analyzing powers for the 0–3.5 MeV energy region (see Sec. IV). The solid lines are the DWBA predictions for the assigned  $J^\pi$ , while dot-dashed (or dashed) lines are experimental  $A_y(\theta)$  distributions of known levels with same  $J^\pi$  (or opposite spin-orbit partner). The dotted line is the spin-orbit partner prediction.

sponding approximately to groups (3+4) and (9+10) of the present work, respectively, with rather comparable  $C^2S$  values.

The third class encompasses the  $A_y(\theta)$ 's of slices 10–12 (5.10–5.45 MeV) and 19 (6.75 MeV), which cross-section and analyzing-power angular distributions are well reproduced by a mixing of  $l=3$  ( $\frac{7}{2}^-$ ) and  $l=1$  ( $\frac{3}{2}^-$ ) transfers assuming the same yield from  $1f_{7/2}$  and  $2p_{3/2}$  contributions.

The last class includes the  $A_y(\theta)$ 's from groups 13–18, corresponding to the excitation energy region 5.45–6.6 MeV. Although the corresponding cross sections are rather well described by the same  $l=3+l=1$  mixing as above, the experimental analyzing powers have a behavior very similar to that of the 1.1 MeV ( $\frac{3}{2}^-$ ) level (see Fig.

5). This striking feature suggests a more significant contribution of the  $l=1$  transfer and, once more, shows the strong sensitivity of analyzing powers to the spin mixing ratio, opposite to the cross-section behavior. Since the 1.1 and 1.87 MeV levels exhaust about 90% of the  $2p_{3/2}$  strength, the missing strength could be partly concentrated in this region. The  $2p_{3/2}$  valence strength appears to be much more fragmented and spread than the  $2p_{1/2}$  or even the  $1g_{9/2}$  strength, and this fragmentation is clearly observed for the first time in the present work. Such a fragmentation of the  $2p_{3/2}$  strength can be related to the various possibilities of weak coupling leading to  $J^\pi = \frac{3}{2}^-$  components.

## VI. SUMMED SPECTROSCOPIC STRENGTHS AND DISTRIBUTION OF NEUTRON HOLE STATES

The summed spectroscopic strengths ( $\sum C^2S$ ) measured for  $l=1,3,4$  transitions are summarized in Table IV with the corresponding centroid energies. The strength distribution of  $l=3$  single neutron hole is displayed in Fig. 6 and compared with the theoretical predictions of the quasiparticle phonon model<sup>11</sup> (QPM) (see also Table IV).

### A. $l=4$ transitions

The main part of the  $1g_{9/2}$   $T_<$  strength (78%) is found to be concentrated in the ground state, as in previous works (Refs. 8–10). Other weak components are observed between 2.6 and 3.5 MeV excitation energy, carrying about 7.3% of the total strength. The 2.28 and 2.39 MeV levels populated via the  $l=4$  transfer are assumed to have a  $J^\pi = \frac{9}{2}^+$  assignment from the  $A_y(\theta)$  data. They could belong, as the  $J^\pi = \frac{5}{2}^+$ ,  $E_x = 1.62$  MeV level, to the ( $1g_{9/2} \times 2^+$ ) multiplet, which is expected, in a pure-coupling scheme, to lie around 2.2 MeV. The centroid of the  $1g_{9/2}$  ( $T_< + T_>$ ) strength, deduced from the present experiment, is 0.40 MeV, to compare with the values of 0.32 MeV (Ref. 9) and 0.43 (Ref. 10) extracted from ( $^3\text{He}, \alpha$ ) experiments.

A comparison with the neighboring  $N=49$  nuclei shows similar features about the fragmentation of the  $1g_{9/2}$  strength, which is also mainly concentrated in the ground state, and to a lesser extent in the second  $\frac{9}{2}^+$  state: In  $^{87}\text{Sr}$  (Ref. 23) and  $^{91}\text{Mo}$  (Ref. 24) the values extracted from ( $^3\text{He}, \alpha$ ) studies are, respectively, 0.45 and 0.42 MeV, close to the corresponding value in  $^{89}\text{Zr}$  (0.40 MeV) deduced from the present ( $\bar{p}, d$ ) study.

### B. $l=1$ transitions

The  $2p_{1/2}$  ( $T_<$ ) strength is found to be concentrated ( $\sim 86\%$  of the total observed yield) in the first known  $\frac{1}{2}^-$  level at 0.595 MeV, but another weak  $2p_{1/2}$  component, previously assumed to be  $2p_{3/2}$ , is clearly identified at 1.75 MeV and carries  $\sim 14\%$  of the total observed strength. The whole  $2p_{1/2}$  strength appears to be fully exhausted by these two levels, the  $C^2S$  value determined for the lowest  $\frac{1}{2}^-$  state already exceeding the  $2p_{1/2}$   $T_<$  sum rule by  $\sim 30\%$ .

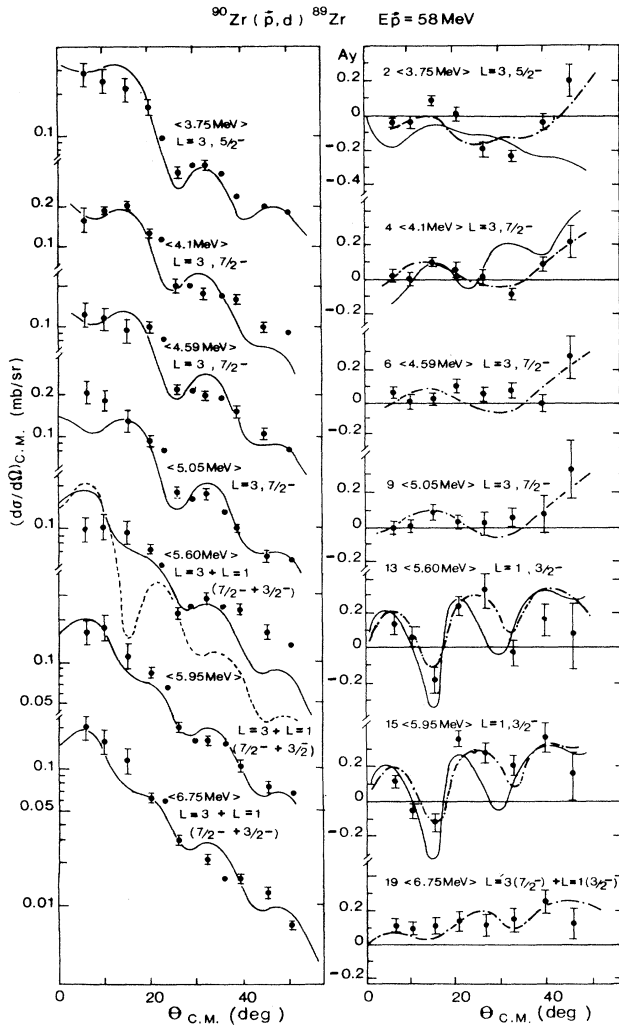


FIG. 5. Typical angular distributions of differential cross sections and analyzing powers for the 3.5–7 MeV energy region (see Sec. V). The caption is the same as Fig. 4. The dashed line is the typical DWBA cross section for  $l=1$  ( $\frac{3}{2}^-$ ).

The  $2p_{3/2}$  ( $T_{<}$ ) strength is found to be much more fragmented and shared between two energy regions. The first one includes the main fragment, at 1.1 MeV, and the 1.87-MeV ( $\frac{3}{2}^-$ ) level, which exhaust 74% and 16%, respectively, of the total measured strength. The missing strength ( $\sim 10\%$ ) appears to be much fragmented and mainly located in the 5.45–6.6-MeV excitation energy range, as clearly demonstrated by the  $A_y(\theta)$  angular distributions recorded in the present experiment. This noticeable concentration of  $p_{3/2}$  strength around 6 MeV can be related to the weak coupling of  $1g_{9/2}$  with the  $3^-$  low

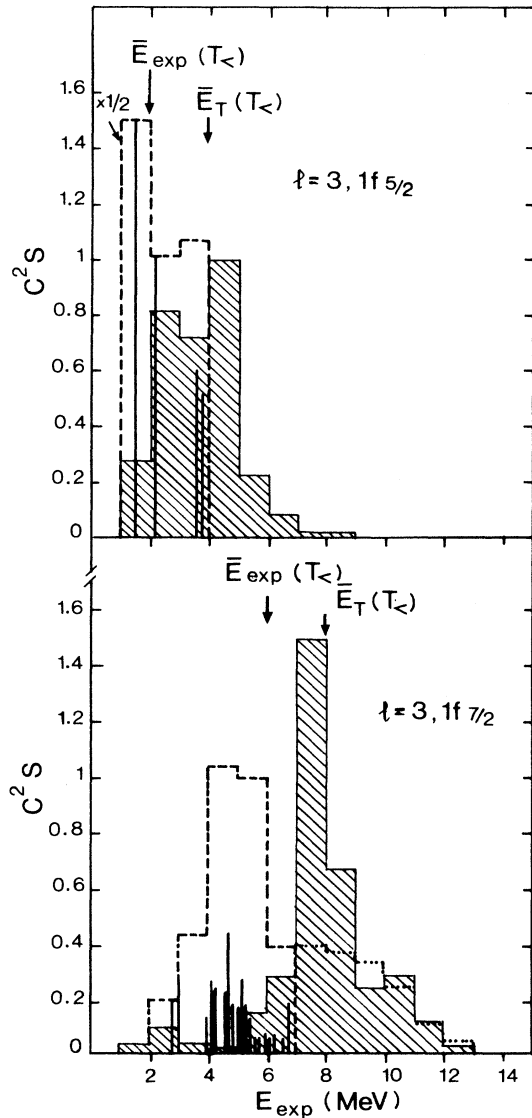


FIG. 6. Distribution of  $l=3$  experimental neutron hole strength relative to excitation energy and comparison with normalized theoretical predictions of Ref. 11 (hatched areas). Above 7 MeV, the  $1f_{7/2}$  experimental results (dotted lines) are taken from Ref. 9. Spectroscopic factors of discrete levels are represented with vertical bars. The  $\bar{E}_{\text{expt}}$  and  $\bar{E}_T$  stand for experimental  $T_{<}$  strength centroids and QPM predictions, respectively.

TABLE IV. Centroid energies and summed spectroscopic factors for valence and inner neutron hole states in  $^{89}\text{Zr}$  and comparison with other works and theoretical predictions.

Neutron orbital	$E_{T_{<}}$ (expt) (MeV)	$\sum C^2 S$	This work $E_j(T_{<}, T_{>})$ (MeV)	$\sum C^2 S$	$(\bar{p}, d)$ at 90 MeV (Ref. 8) $E_j(T_{<}, T_{>})$ (MeV)	$\sum C^2 S$	$(^3\text{He}, \alpha)$ at 97 MeV (Ref. 9) $E_j(T_{<}, T_{>})$ (MeV)	$\sum C^2 S$	$(^3\text{He}, \alpha)$ at 39 MeV (Ref. 10) $E_j$ (MeV)	Theory (Ref. 11) $E_j$ (MeV)	$C^2 S$
valence shells (0–7 MeV)											
$1g_{9/2}$	0.34 <sup>a</sup>	8.2 <sup>a</sup>	0.40 <sup>a</sup>	8.26 <sup>a</sup>	0.18	10.0	0.32	9.8	0.43	(0–10 MeV)	9.2
$2p_{1/2}$	0.753	2.77	1.11	2.91	1.23	1.31	1.00	1.8	1.28		1.9
$2p_{3/2}$	1.24	3.59	2.14	3.81	1.95	2.87	2.11	3.7	2.01		3.8
$1f_{5/2}$	2.05	5.17	2.91	5.58	3.27	6.96	2.86	5.4	2.95		5.5
inner shell (0–7 MeV)											
$1f_{7/2}$	4.71	3.45 <sup>c</sup>	9.02 <sup>b</sup>	8.78 <sup>b</sup>	10.3	6.50	7.20	5.6	5.2	(0–13 MeV)	5.2
			7.44 <sup>d</sup>	5.85 <sup>d</sup>		1.17 <sup>e</sup>		3.6 <sup>e</sup>	8.3	(0–14 MeV)	7.8
											(3.48 <sup>f</sup> )

<sup>a</sup>Including contribution of unresolved 1.52 MeV ( $\frac{3}{2}^+$ ) level with  $C^2 S \approx 0.37$  as estimated in Ref. 10.

<sup>b</sup>Adopting  $C^2 S$  values of Ref. 8 for  $E_x = 7-21$  MeV.

<sup>c</sup>Assuming the same yield from  $2p_{3/2}$  and  $1f_{7/2}$  at forward angles for the energy bins 13–18 (5.5–6.6 MeV).

<sup>d</sup>Adopting  $C^2 S$  values of Ref. 9 for  $E_x = 7-19$  MeV.

<sup>e</sup>If  $E_x$  interval is (0–7 MeV),  $T_{<}$  components only.

<sup>f</sup>If  $E_x$  interval is (0–12 MeV),  $T_{<}$  components only.

energy octupole resonance (LEOR) of  $^{90}\text{Zr}$  located at  $E_x = 7.2$  MeV.<sup>26</sup>

The centroids of  $2p_{1/2}$  and  $2p_{3/2}$  ( $T_< + T_>$ ) strengths, deduced from the present study, are, respectively, 1.11 and 2.14 MeV, which compare very closely with the values of 1.23–1.95 MeV,<sup>8</sup> 1.0–2.11 MeV,<sup>9</sup> and 1.28–2.01 MeV,<sup>10</sup> extracted from ( $\bar{p}, d$ ) or ( $^3\text{He}, \alpha$ ) experiments (see Table IV). The corresponding  $2p$  spin-orbit splitting values are 1.03 MeV (present work), 0.72 MeV,<sup>8</sup> 1.11 MeV,<sup>9</sup> and 0.73 MeV,<sup>10</sup> to be compared to the value of 1.78 MeV deduced from Hartree-Fock calculations.<sup>25</sup>

In the neighboring  $N=49$  nuclei,<sup>23,24</sup> similar strong fragmentation of the  $2p_{3/2}$  remaining strength is suggested. In  $^{87}\text{Sr}$ , for example,<sup>23</sup> most of the  $l=1$  levels observed between 2 and 6 MeV, and the  $2p$  strength identified in the high-energy continuum up to 12 MeV, are assumed to be  $J^\pi = \frac{3}{2}^-$ , the first low-lying  $\frac{1}{2}^-$  state already exhausting the  $2p_{1/2}$   $T_<$  sum rule by  $\sim 36\%$ .

### C. $l=3$ transitions

The  $1f_{5/2}$   $T_<$  hole strength is mainly exhausted in the first two known  $\frac{5}{2}^-$  levels at 1.46 MeV (55%) and 2.11 MeV (20%). Most of the remaining strength ( $\sim 19\%$ ) is found to be shared between the two levels at 3.57 and 3.75 MeV, which were unambiguously assigned  $J^\pi = \frac{5}{2}^-$  in the present work. Then the  $1f_{5/2}$   $T_<$  hole strength is practically fully exhausted below 3.9 MeV excitation energy, allowing us to give a reliable estimation of the centroid of  $1f_{5/2}$  ( $T_<, T_>$ ) neutron hole strength. The value deduced from the present work is 2.91 MeV, very close to the values given in Ref. 9,  $E_j(T_<, T_>) = 2.86$  MeV, or in Ref. 10,  $E_j = 2.95$  MeV, but lower than the value of 3.27 MeV deduced from the  $^{90}\text{Zr}(\bar{p}, d)^{89}\text{Zr}$  experiment at 90 MeV.<sup>8</sup> In this latter study, a larger part ( $\sim 25\%$ ) of the observed  $1f_{5/2}$   $T_<$  strength is found to be located in the 3.4–7.0-MeV region, which leads to a larger  $C^2S$  and therefore to an overestimate of the corresponding centroid value, and moreover leads to exhaust the total sum rule (see Table IV). It must be noted that in the neighboring nucleus  $^{87}\text{Sr}$ , the  $1f_{5/2}$   $T_<$  centroid value extracted from the ( $^3\text{He}, \alpha$ ) experiment<sup>23</sup> is 2.4 MeV, assuming that all the  $1f_{5/2}$   $T_<$  strength is exhausted below 5 MeV.

Turning now to the  $1f_{7/2}$  orbital, the two weak components identified below 3.5 MeV, at 2.78 and 3.02 MeV, carry  $\sim 7\%$  of the  $1f_{7/2}$   $T_<$  strength. Almost the whole structure extending from 3.5 to 7 MeV is found to be mainly populated via  $1f_{7/2}$  pickup (apart from the  $2p_{3/2}$  concentration in the 5.45–6.6 MeV range, as explained above), and carries  $\sim 40\%$  of the total  $1f_{7/2}$   $T_<$  sum rule. Such a value is quite different from the 16% deduced from the ( $\bar{p}, d$ ) experiment at 90 MeV.<sup>8</sup> This discrepancy may be due in part to their global analysis of the 3.5–7 MeV structure, which does not allow accurate separation of the  $1f_{5/2}$  and  $1f_{7/2}$  respective contributions, and to a possible overestimation in our data of the  $1f_{7/2}$  contribution in the region of  $2p_{3/2}$  concentration. In summary our results indicate that  $\sim 50\%$  of the  $1f_{7/2}$   $T_<$  strength lies in the 0–7 MeV region, with strong con-

centration ( $\sim 40\%$ ) in the 3.5–7 MeV bump. The corresponding energy centroid of the observed  $T_<$  strength is 4.71 MeV, in agreement with the values given in Ref. 10 (5.20 MeV) and Ref. 9 (4.9 MeV). The missing  $1f_{7/2}$   $T_<$  strength ( $\sim 50\%$ ) located at higher excitation energies, as observed in previous ( $^3\text{He}, \alpha$ ) (Ref. 9) or ( $\bar{p}, d$ ) (Ref. 8) experiments is out the scope of this study. So the  $1f_{7/2}$  strength appears to be more widely spread than the  $1f_{5/2}$  one, with no sharp level comparable to the 1.46 MeV ( $\frac{5}{2}^-$ ) one.

A comparison with the  $N=49$  neighboring nuclei shows that in  $^{87}\text{Sr}$  (Ref. 23) and  $^{91}\text{Mo}$  (Ref. 24) only 21% and 14%, respectively, of the  $1f_{7/2}$   $T_<$  strength lies below 7 MeV. These values are appreciably lower than the 50% observed in the present work, but it must be noted that these two ( $^3\text{He}, \alpha$ ) experiments were not able to discriminate between  $1f_{5/2}$  and  $1f_{7/2}$  strengths, leading to a possible underestimation of the observed  $1f_{7/2}$  strength.

Theoretical calculations performed in the frame of the quasiparticle phonon coupling model<sup>11</sup> predict the distribution of  $1f_{5/2}$  and  $1f_{7/2}$  neutron hole strengths in  $^{89}\text{Zr}$  and  $^{91}\text{Mo}$ . In the  $^{89}\text{Zr}$  nucleus (see Fig. 6), the  $1f_{5/2}$  strength is predicted to be at higher excitation energy than experiment shows. The calculated energies of the two first  $\frac{5}{2}^-$  states are higher ( $\sim 0.7$  MeV) than the experimental ones with spectroscopic factors smaller than observed. Moreover, the first  $\frac{5}{2}^-$  level is predicted to be weaker than the second one, opposite to the experimental situation. The remaining  $1f_{5/2}$   $T_<$  strength ( $\sim 55\%$ ) is predicted to be distributed from 3.5 to 9 MeV, the  $J^\pi = \frac{5}{2}^-$  states giving the main contribution to the cross section in the interval  $3.5 \leq E_x \leq 5$  MeV. However, the present data indicate that no significant  $1f_{5/2}$   $T_<$  component is identified above 4 MeV, the last part of the  $1f_{5/2}$  strength ( $\sim 17\%$ ) being observed in the interval  $3 \leq E_x \leq 4$  MeV. Therefore, the calculated centroid of the  $1f_{5/2}$   $T_<$  strength distribution is  $E_x = 3.8$  MeV, higher than the experimental value  $E_x = 2.05$  MeV.

Turning now to the  $1f_{7/2}$  strength, the calculations predict that its main part should be distributed above  $E_x = 7$  MeV, with strong concentration ( $\sim 60\%$ ) from 7 to 9 MeV, only  $\sim 20\%$  being exhausted below  $E_x = 7$  MeV. However, our data show that the main contribution to the cross section in the interval  $4 \leq E_x \leq 7$  MeV is due to  $1f_{7/2}$  neutron pickup, with local concentration ( $\sim 30\%$ ) at  $E_x \simeq 4\text{--}5.4$  MeV. A minimum of about 45% of the  $T_<$  strength is found below  $E_x = 7$  MeV, which is somewhat different from predictions, as clearly shown on Fig. 6.

If experimental  $C^2S$  values from the ( $\bar{p}, d$ ) study at 90 MeV (Ref. 8) are adopted for  $E_x = 7\text{--}21$  MeV, the centroid of the  $1f_{7/2}$  ( $T_<, T_>$ ) strength should be  $E_x = 9.02$  MeV, and the experimental deduced spin-orbit splitting of the  $1f$  neutron shell  $\mathcal{E}_{s.o.}^n(1f)$  should be equal to 6.1 MeV. Choosing the  $C^2S$  values of the ( $^3\text{He}, \alpha$ ) experiment<sup>9</sup> for  $E_x = 7\text{--}19$  MeV leads to a centroid energy of 7.44 MeV and to a corresponding  $\mathcal{E}_{s.o.}^n(1f)$  value of 4.53 MeV very close to the QPM predicted value  $\mathcal{E}_{s.o.}^n = 4.5$

MeV (Ref. 11) or to the value (4.93 MeV) extracted from Hartree-Fock calculations.<sup>25</sup> These experimental values of the spin-orbit splitting are rather close to the experimental  $1f$  proton splitting in the  $^{89}\text{Y}$  parent nucleus ( $\mathcal{E}_{s.o.}^p = 5.1$  MeV),<sup>27</sup> or even in other neighboring nuclei [ $\mathcal{E}_{s.o.}^p = 5.5$  MeV (Ref. 28) and  $\mathcal{E}_{s.o.}^n = 5.3$  MeV (Ref. 23)].

## VII. SUMMARY AND CONCLUSIONS

The present investigation of the  $^{90}\text{Zr}(\bar{p}, d)^{89}\text{Zr}$  reaction with good energy resolution has allowed, through analyzing-power measurements, spin and parity assignments for valence states as well as for inner-lying hole states, up to 7 MeV excitation energy where fine structures are still observed.

This study establishes firmly the fragmentation of the  $1g_{9/2}$ ,  $2p_{1/2}$ , and  $2p_{3/2}$  valence neutron hole strengths in  $^{89}\text{Zr}$ . The main part ( $\geq 74\%$ ) of each related  $T_{<}$  hole strength is concentrated in the corresponding first low-lying level.

The remaining  $1g_{9/2}$  strength is found to be distributed over several small fragments up to  $E_x \approx 3.5$  MeV. The  $2p_{1/2}$  missing strength is concentrated in only one low-lying level at 1.75 MeV. In contrast, the missing part of the  $2p_{3/2}$  strength appears to be much more fragmented and spread over a large excitation energy range. In addition to the 1.87 MeV component unambiguously assigned  $J^\pi = \frac{3}{2}^-$ , a concentration of several  $2p_{3/2}$  fragments, carrying  $\sim 10\%$  of the single-particle strength, is clearly identified for the first time between  $\sim 5.2$  and  $\sim 6.8$  MeV.

Half of the total  $1f_{5/2}$   $T_{<}$  strength is concentrated in the 1.46 MeV level, the remaining part being mostly distributed over three fragments at 2.11, 3.57, and 3.75 MeV. Thus the  $1f_{5/2}$   $T_{<}$  strength appears to be practically exhausted below  $E_x \approx 3.8$  MeV, as suggested in the previous ( $^3\text{He}, \alpha$ ) experiments,<sup>9,10</sup> but in contrast with the  $(\bar{p}, d)$  study<sup>8</sup> where substantial  $1f_{5/2}$  strength ( $\sim 30\%$ ) was observed between 3.4 and 7.0 MeV.

On the other hand, the present data show that the numerous fine structures observed between  $\sim 3.4$  and  $\sim 7.0$  MeV are mainly due to the excitation of  $1f_{7/2}$  inner hole orbital and carry  $\sim 40\%$  of the strength. In-

cluding the small  $1f_{7/2}$  components identified below 3.4 MeV, only  $\sim 50\%$  of the  $1f_{7/2}$   $T_{<}$  strength is found to be exhausted in the 2.5–7 MeV region, which confirms the results of the ( $^3\text{He}, \alpha$ ) experiments.<sup>9,10</sup> The  $1f_{7/2}$  strength appears definitely much more widely spread than the  $1f_{5/2}$  one, with no sharp level comparable to the strongly populated 1.46 MeV  $\frac{5}{2}^-$  state.

The  $1f$  neutron spin-orbit splitting value deduced from our data is rather close to the ones obtained for neighboring and parent nuclei, and also to the value calculated with standard parameters of the phenomenological Saxon-Woods (SW) potential used in QPM predictions.<sup>11</sup> However, the  $1f$  theoretical strength distributions do not reproduce the experimental ones: the  $1f_{5/2}$  strength is predicted to be much more fragmented than observed (in particular, the dominant fragment at 1.46 MeV is not reproduced); furthermore, the  $1f_{7/2}$  strength is predicted to be less fragmented and mainly distributed above  $E_x \approx 7$  MeV, with  $\sim 80\%$  of the strength lying between  $\sim 7$  and  $\sim 12.3$  MeV. Moreover, the energy centroids of the experimental  $2p$  and  $1f_{5/2}$  strength distributions are closer to each other and to the ground state than the corresponding single-hole energies of Ref. 11. On the other hand, these experimental values are in good agreement with the energies of  $2p_{1/2}$ ,  $2p_{3/2}$ , and  $1f_{5/2}$  neutron hole states which were adjusted to correctly describe the low-lying levels of  $N=49$  isotones by taking into account in a semimicroscopic model the coupling of neutron holes with quadrupole and octupole vibrations of the even-even core.<sup>29</sup> The most probable reason for the disagreement of the QPM predictions with the present experimental results could be the choice of the SW parameters. Comparing our data with the results of Ref. 11 definitely proves that it is necessary to check these parameters more carefully. More refined calculations are required to reproduce in the same framework not only the  $1f$  inner strength distribution, but also the  $1g_{9/2}$  and  $2p$  valence ones.

We would like to thank Professor A. I. Vdovin for very fruitful discussions.

<sup>1</sup>S. Galès, in *Proceedings of the Niels Bohr Symposium on Nuclear Structure*, edited by R. Broglia, G. B. Hagemann, and B. Herskind (Elsevier, Amsterdam, 1985), p. 57, and references therein; S. Galès, in *Lectures at the International School on Nuclear Structure Alhusta, URSS, 1985*, edited by V. G. Soloviev and Y. P. Popov (unpublished), p. 51, and references therein; S. Galès, Ch. Stoyanov, and A. I. Vdovin, *Phys. Rep.* **166**, 127 (1988), and references therein.  
<sup>2</sup>A. Stuirbrink, G. J. Wagner, K. T. Knopfle, Liu Ken Pao, G. Mairle, H. Riedesel, and K. Schindler, *Z. Phys. A* **297**, 307 (1980).  
<sup>3</sup>K. Reiner, P. Grabmayr, G. J. Wagner, S. M. Banks, B. G. Lay, V. C. Officer, G. G. Schute, B. M. Spicer, C. W. Glover, W. P. Jones, D. W. Miller, H. Nann, and E. J. Stephenson, *Nucl. Phys.* **A472**, 1 (1987).  
<sup>4</sup>G. M. Crawley, J. Kasagi, S. Galès, E. Gerlic, D. Friesel, and

A. Bacher, *Phys. Rev. C* **23**, 1818 (1981).  
<sup>5</sup>G. Perrin, G. Duhamel, C. Perrin, E. Gerlic, S. Galès, and V. Comparat, *Nucl. Phys.* **A356**, 61 (1981).  
<sup>6</sup>S. Galès, E. Gerlic, G. Duhamel, G. Perrin, C. Perrin, and V. Comparat, *Nucl. Phys.* **A381**, 40 (1982).  
<sup>7</sup>R. H. Siemssen, C. C. Foster, W. W. Jacobs, W. P. Jones, D. W. Miller, M. Saber, and F. Soga, *Nucl. Phys.* **A405**, 205 (1983).  
<sup>8</sup>J. Kasagi, G. M. Crawley, A. Kashy, J. Duffy, S. Galès, E. Gerlic, and D. Friesel, *Phys. Rev. C* **28**, 1065 (1985).  
<sup>9</sup>G. Duhamel, G. Perrin, J. P. Didelez, E. Gerlic, H. Langevin-Joliot, J. Guillot, and J. Van de Wiele, *J. Phys. G* **7**, 1415 (1981).  
<sup>10</sup>S. Galès, E. Hourani, S. Fortier, H. Laurent, J. M. Maison, and J. P. Schapira, *Nucl. Phys.* **A288**, 221 (1977).  
<sup>11</sup>N. D. Thao, V. G. Soloviev, Ch. Stoyanov, and A. I. Vdovin,

- J. Phys. G **10**, 517 (1984).
- <sup>12</sup>P. Martin, Y. Gaillard, P. de Saintignon, G. Perrin, J. Chauvin, G. Duhamel, and J. M. Loiseaux, Nucl. Phys. **A315**, 291 (1979).
- <sup>13</sup>P. D. Kunz, University of Colorado Report No. C00-535-606, 1975.
- <sup>14</sup>C. M. Perey and F. G. Perey, Nucl. Data Tables **16**, 65 (1976).
- <sup>15</sup>K. Hatanaka, K. Imai, S. Kobayashi, T. Matsusue, M. Nakamura, K. Nisimura, T. Noro, H. Sakamoto, H. Shimizu, and J. Shirai, Nucl. Phys. **A340**, 93 (1980).
- <sup>16</sup>G. Mairle, K. T. Knopfle, H. Riedesel, G. J. Wagner, H. Bechtold, and L. Friedrich, Nucl. Phys. **A339**, 61 (1980).
- <sup>17</sup>K. Hosono, M. Kondo, T. Saito, N. Matsukoa, S. Nagamachi, T. Noro, H. Shimizu, S. Kato, K. Okada, K. Ogino, and Y. Kadota, Nucl. Phys. **A343**, 234 (1980).
- <sup>18</sup>J. J. Menet, E. E. Gross, J. J. Malanafy, and A. Zucker, Phys. Rev. C **4**, 1114 (1971).
- <sup>19</sup>F. D. Bechetti and G. W. Greenless, Phys. Rev. **182**, 1190 (1969).
- <sup>20</sup>R. G. Johnson and P. J. Soper, Phys. Rev. C **1**, 976 (1970).
- <sup>21</sup>M. Matoba, H. Ijiri, H. Kametani, T. Sakae, H. Kurowaka, K. Komatsu, I. Kumabe, M. Hyakutake, N. Koori, and T. Maki, R.C.N.P. Annual Report No. 19, 1982.
- <sup>22</sup>Nucl. Data Sheets **58**, 351 (1989), and references herein.
- <sup>23</sup>S. Fortier, S. Galès, E. Hourani, J. M. Maison, C. P. Massolo, and J. P. Schapira, Phys. Rev. C **39**, 82 (1989).
- <sup>24</sup>C. P. Massolo, S. Fortier, J. M. Maison, and M. N. Rao, J. Phys. G **8**, 361 (1982).
- <sup>25</sup>M. Beiner, H. Flocard, N. Van Giai, and P. Quentin, Nucl. Phys. **A238**, 29 (1975).
- <sup>26</sup>J. M. Moss, D. R. Brown, D. H. Youngblood, C. M. Rozsa, and J. D. Bronson, Phys. Rev. C **18**, 741 (1978).
- <sup>27</sup>A. Stuirbrink, G. J. Wagner, K. T. Knopfle, Ken Pao Liu, G. Mairle, H. Riedesel, K. Schindler, V. Bechtold, and L. Friedrich, Z. Phys. A **297**, 307 (1980).
- <sup>28</sup>A. Pfeiffer, G. Mairle, K. T. Knopfle, P. Grabmayr, G. J. Wagner, V. Bechtold, and L. Friedrich, Nucl. Phys. **A455**, 381 (1986).
- <sup>29</sup>S. K. Basu and S. Sen, Nucl. Phys. **A220**, 580 (1974).